

PAPIR: Practical RIS-aided Localization via Statistical User Information

Antonio Albanese^{*†}, Placido Mursia^{*}, Vincenzo Sciancalepore^{*}, Xavier Costa-Pérez^{*‡}

^{*}NEC Laboratories Europe, Heidelberg, Germany

[†]Departamento de Ingeniería Telemática, University Carlos III of Madrid, Leganés, Spain

[‡]i2cat Foundation and ICREA, Barcelona, Spain

{name.surname}@neclab.eu

Abstract—The integration of advanced localization techniques in the upcoming next generation networks (5G/6G) is becoming increasingly important for many use cases comprising contact tracing, natural disasters, terrorist attacks, etc. Therefore, emerging lightweight and passive technologies that allow accurately controlling the propagation environment, such as *reconfigurable intelligent surfaces (RISs)*, may help to develop advance positioning solutions relying on channel statistics and beamforming. In this paper, we devise PAPIR, a practical localization system leveraging on RISs by designing a two-stage solution building upon prior statistical information on the target user equipment (UE) position. PAPIR aims at finely estimating the UE position by performing statistical beamforming, direction-of-arrival (DoA) and time-of-arrival (ToA) estimation on a given three-dimensional search space, which is iteratively updated by exploiting the likelihood of the UE position.

Index Terms—RIS, DoA estimation, ToA estimation, Statistical beamforming, RIS-aided localization.

I. INTRODUCTION

The radio environment represents the main propagation means that has been deeply analyzed to make wireless communications efficient and reliable. In particular, such a black-box model has been lumped together with advance coding solutions to properly tackle uncontrolled fading issues while still facilitating reasonably-stable channels. Recently, reconfigurable intelligent surfaces (RISs) appear as the revolutionary and emerging technology bringing the ability of controlling—with passive devices—such propagation environment, via, e.g., backscattering or phase-shifting the incoming electromagnetic waves: this overcomes the traditional adversary perception of the channel thereby turning it into an optimization variable and, in turn, tunable parameter [1]–[5].

Manipulating the geometry of the radio propagation has recently drawn vast interest in the scientific community for the design of localization and mapping solutions [6]–[9]. State-of-the-art RIS-aided localization employs RISs in two alternative ways: *i*) receive mode [10], namely provided with a limited number of RF chains, and *ii*) reflection mode [11]. The former techniques aim at localizing a target user equipment (UE) fronting the RIS, e.g., by leveraging on the near-field wavefront curvature [12]. Whereas, the latter category builds upon the reconfigurability of the RISs by suitably optimizing the reflection coefficients and allowing a fully passive RIS design, which is arguably their most attractive operational

mode. Indeed, this allows lightening the manufacturing cost and boiling down the overall complexity as well as maximizing deployment flexibility. In this regard, RISs can deliver remarkable improvements of one order of magnitude in terms of position error bound (PEB) with respect to a non-RIS scenario, given a proper phase design [13]. Moreover, a RIS provides better PEB and orientation error bound (OEB) than a single scatter point [14].

Existing RIS-aided reflection mode localization algorithms leverage on direct maximum-likelihood estimate of the UE position, which is known to be computationally expensive [13], or fingerprinting solutions based on received signal strength (RSS) measurements at the UE-side. Indeed, RISs can exacerbate the RSS differences among different locations, thus improving the localization accuracy [15]. In this regard, the performance of fingerprinting can be enhanced by the aid of machine learning (ML) techniques via feature selection, which prunes the large state space of the RIS and reduces the overall complexity of the position estimation [16]. However, the above-mentioned techniques lack of practical assumptions on the unknown UE location. Since proper phase shift configuration of RISs operating in reflection mode requires the UE position, which is exactly the quantity to be estimated, a chicken-egg problem raises.

In this paper, we propose a novel two-stage RIS-aided localization algorithm denoted as PAPIR, namely PAssive PosItioning with RIS, which retrieves the time-of-arrival (ToA) and the direction-of-arrival (DoA) of reference signals sent by the UE to estimate its position. We assume the RIS to be in reflection mode and we optimize its reflection coefficients based on some (possibly) coarse prior information on the UE position. To the best of our knowledge, this is the first work presenting a practical and efficient solution able to localize a UE with realistic assumptions on its position. We present a thorough numerical evaluation to assess the performance of the proposed scheme in terms of localization accuracy.

Notation. We use \mathbb{C}^n and $\mathbb{C}^{m \times n}$ to represent the sets of n -dimensional complex vectors and $m \times n$ complex matrices, respectively. Vectors are denoted by default as column vectors. We let $(\cdot)^H$, $(\cdot)^T$, and $(\cdot)^*$ to denote the Hermitian, transpose, and conjugate operators, respectively. $\|\cdot\|$ is the L2-norm of a vector, whereas \mathbf{I}_N and \otimes are the N -dimensional identity matrix and the Kronecker product, respectively.

II. SYSTEM MODEL

We consider the scenario depicted in Fig. 1 where an access point (AP) equipped with M antennas performs the localization of a target single-antenna UE with the aid of a RIS consisting of N elements. Specifically, the UE transmits uplink reference signals to the AP who then processes the received signal and estimates the UE position. We model the AP as a uniform linear array (ULA) with M antennas along the x and y axis, respectively, with $N = N_x N_y$. The AP is located at the origin of our reference system and the RIS array center has coordinates $\mathbf{p}_R \in \mathbb{R}^3$, while only a given probability distribution function (pdf) of the position of the UE $\mathbf{p} \in \mathbb{R}^3$ is known and given by $f_p(\mathbf{p})$. We assume that there is no direct link between the UE and the AP, so that communication between the two must be established via the path reflected upon the RIS. The latter is decomposed into the line-of-sight (LoS) channel $\mathbf{h}(\mathbf{p}) \in \mathbb{C}^N$ through which the RIS reflects the impinging signal towards the AP for a given UE position \mathbf{p} , and the AP-RIS LoS link denoted by $\mathbf{G} \in \mathbb{C}^{N \times M}$. We assume that all channels follow a quasi-static flat-fading model and thus remain constant over the transmission time of the reference signals. Moreover, we employ millimeter wave frequencies, which are characterized by sparse multipath even in complex propagation conditions such as dense urban or indoor environments. Let ψ_D and ψ_A indicate the angle of departure (AoD) from the RIS and the angle of arrival (AoA) at the AP, respectively. Hence, the LoS RIS-AP channel \mathbf{G} is defined as

$$\mathbf{G} \triangleq \sqrt{\gamma_G} \mathbf{b}(\psi_D) \mathbf{a}(\psi_A)^H, \quad (1)$$

where $\gamma_G \triangleq d_G^{-\beta}$ is the channel power gain with d_G the distance between the RIS and the AP and β the pathloss exponent, $\mathbf{b}(\psi_D) \in \mathbb{C}^N$ is the PLA response vector at the RIS for the steering angle ψ_D , and $\mathbf{a}(\psi_A) \in \mathbb{C}^M$ is the ULA response vector at the AP for the steering angle ψ_A . The former is given by

$$\begin{aligned} \mathbf{b}(\psi_D) &\triangleq \mathbf{b}_z(\psi_{D,z}, \psi_{D,x}) \otimes \mathbf{b}_x(\psi_{D,z}, \psi_{D,x}) \\ &= [1, e^{j2\pi\delta \sin(\psi_{D,z}) \cos(\psi_{D,x})}, \dots, \\ &\quad e^{j2\pi\delta(N_y-1) \sin(\psi_{D,z}) \cos(\psi_{D,x})}]^T \\ &\quad \otimes [1, e^{j2\pi\delta \sin(\psi_{D,x}) \cos(\psi_{D,z})}, \dots, \\ &\quad e^{j2\pi\delta(N_x-1) \sin(\psi_{D,x}) \cos(\psi_{D,z})}]^T, \end{aligned} \quad (2)$$

where $\psi_{D,z}$ and $\psi_{D,x}$ are the azimuth and elevation AoD, respectively, and $\delta = 0.5$ is the antenna spacing-wavelength ratio. In a similar way, the ULA response at the AP is defined as

$$\mathbf{a}(\psi_A) \triangleq [1, e^{j2\pi\delta \cos(\psi_A)}, \dots, e^{j2\pi\delta(M-1) \cos(\psi_A)}]^T. \quad (4)$$

Note that the coordinates of the RIS position $\mathbf{p}_R = [p_{R,x}, p_{R,y}, p_{R,z}]^T$ are expressed as $p_{R,x} = \|\mathbf{p}_R\| \cos(\psi_{D,z}) \cos(\psi_{D,x})$, $p_{R,y} = \|\mathbf{p}_R\| \cos(\psi_{D,z}) \sin(\psi_{D,x})$, and $p_{R,z} = \|\mathbf{p}_R\| \sin(\psi_{D,z})$, respectively. The UE-RIS channel for a given (unknown) UE position \mathbf{p} reads as

$$\mathbf{h}(\mathbf{p}) \triangleq \sqrt{\gamma} \mathbf{b}(\theta), \quad (5)$$

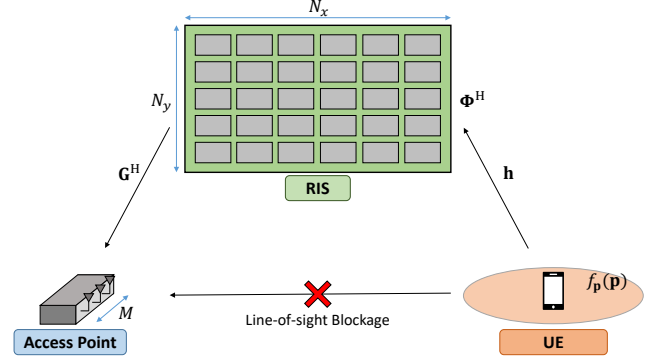


Fig. 1: Localization scenario

where $\gamma \triangleq d^{-\beta}$ is the channel power gain with $d = \|\mathbf{p}_R - \mathbf{p}\|$ the Euclidean distance between the UE and the RIS, and $\mathbf{b}(\theta)$ is the PLA response vector of the RIS for the steering angle θ , i.e., the AoA of the LoS UE-RIS path, as in Eq. (2). Note that both d and θ are random variables, which are obtained via proper transformation of the UE position \mathbf{p} , and are thus characterized by the pdf of the UE distribution $f_p(\mathbf{p})$.

The received uplink signal at the AP in time slot n is thus defined as

$$\mathbf{y}(\mathbf{p}, n) \triangleq \sqrt{P} \mathbf{G}^H \mathbf{\Phi}(n) \mathbf{h}(\mathbf{p}) s(n) + \mathbf{n}(n) \in \mathbb{C}^M, \quad (6)$$

where P is the transmit power at the UE, $\mathbf{\Phi}(n) = \text{diag}[\alpha_1(n)e^{j\phi_1(n)}, \dots, \alpha_N(n)e^{j\phi_N(n)}]$ with $\phi_i(n) \in [0, 2\pi]$ and $|\alpha_i(n)|^2 \leq 1, \forall i$ indicates the phase shifts and amplitude attenuation introduced by the RIS in time slot n (to be optimized), while $s(n) \in \mathbb{C}$ is the (known) transmit signal with $|s(n)|^2 = 1, \forall n$, and $\mathbf{n}(n) \in \mathbb{C}^M$ is the additive white Gaussian noise term distributed as $\mathcal{CN}(0, \sigma^2 \mathbf{I}_M), \forall n$. For the sake of simplicity, we assume that the reflections at the RIS are ideal, i.e., that the amplitude attenuations $\{\alpha_i(n)\}_{i=1}^N$ and the phase shifts $\{\phi_i(n)\}_{i=1}^N$ can be independently optimized¹. Lastly, we define the received sum signal-to-noise ratio (SNR) at the AP antennas in time slot n as

$$\text{SNR}(\mathbf{p}, n) \triangleq P \frac{\|\mathbf{G}^H \mathbf{\Phi}(n) \mathbf{h}(\mathbf{p})\|^2}{\sigma^2}, \quad (7)$$

where \mathbf{G} is fully defined by knowing the coordinates of the AP and the RIS as per Eq. (1), $\mathbf{\Phi}$ is set during the RIS optimization phase and \mathbf{h} is a byproduct of the localization procedure.

III. RIS-AIDED LOCALIZATION

Given the model for the channel between the UE and the RIS in Eq. (5), the problem of determining the UE location reduces to the estimation of the steering angle θ and the distance from the RIS d . In this paper, we propose to suitably configure the RIS to reflect the incoming signal from the UE to the AP, who then performs DoA estimation to determine θ ,

¹In real prototypes, amplitude attenuations and phase shifts are dependent and affect the RIS beamforming performance [17]. However, this issue is out of the scope of this work.

and ToA estimation to obtain d . In this respect, we optimize the RIS configuration $\Phi(n)$ at each time slot n in order to maximize the SNR at the AP antennas in Eq. (7) for any given position of the target UE \mathbf{p} . Notably, \mathbf{p} is exactly the quantity we aim at estimating to perform the localization of the UE, thus giving rise to a chicken-egg problem. Therefore, we exploit the prior statistical information about the UE position, which is given by $f_p(\mathbf{p})$, and design an efficient iterative algorithm, denoted as PAPIR, aiming at obtaining a RIS configuration that is robust against the uncertainty in the UE position. Specifically, we adopt the minimum received SNR among the possible UE positions as objective function.

A. DoA Estimation

The task of optimizing the RIS configuration for any given pdf of the UE position $f_p(\mathbf{p})$ is particularly challenging. Indeed, $f_p(\mathbf{p})$ provides only coarse information on the desired direction of reflection at the RIS, thus leading to low received SNR and ultimately poor estimation accuracy. To circumvent this problem, we propose to divide the total three-dimensional area of possible UE positions $\mathcal{A}^{(n)}$ identified by $f_p(\mathbf{p})$ into a set of N_A subareas $\{\mathcal{A}_1^{(n)}, \dots, \mathcal{A}_{N_A}^{(n)}\}$ of equal size $|\mathcal{A}^{(n)}|/N_A$ with a given degree of overlap Δ between two adjacent areas such that

$$\mathcal{A}^{(n)} = \bigcup_{\ell=1}^{N_A} \mathcal{A}_\ell^{(n)}. \quad (8)$$

The AP probes each of the subareas by suitably configuring the RIS, thus producing N_A DoA estimates $\{\hat{\theta}_1, \dots, \hat{\theta}_{N_A}\}$. The AP then defines the next probing space $\mathcal{A}^{(n+1)}$ as the area defined by the union of the subareas corresponding to the $N_A - 1$ DoA estimates that maximize the likelihood of the UE position, which is defined by the pdf $f_p(\mathbf{p})$.² This procedure is repeated until the difference among the DoA estimates of two consecutive iterations of PAPIR is less than a given threshold ϵ . Note that both ϵ and N_A regulate a trade-off between accuracy and estimation time and thus need to be properly designed. Let $f_p^{(n)}(\mathbf{p})$ be the pdf of UE positions corresponding to $\mathcal{A}_\ell^{(n)}$, with $\ell = n \bmod N_A$. Hence, at each time slot n , the RIS is configured to maximize the minimum SNR among the possible UE positions in the area identified by $f_p^{(n)}(\mathbf{p})$, which decreases in size between consecutive probing spaces. This allows us to perform increasingly more selective beamforming, which will give rise to a very sharp increase in SNR when the RIS is pointing in the direction of the UE, compared to when it is pointing in the incorrect direction.

Let us focus on a specific time slot n : here, to ease the notation we drop the time index n and we define $\mathbf{v} \triangleq [\alpha_1 e^{-j\phi_1}, \dots, \alpha_N e^{-j\phi_N}]^T$, with $\Phi = \text{diag}(\mathbf{v}^H)$, and the equivalent uplink channel $\mathbf{H}(\mathbf{p}) \triangleq \text{diag}(\mathbf{h}(\mathbf{p})^H) \mathbf{G}$ such that we can reformulate the SNR in Eq. (7) as

$$\text{SNR}(\mathbf{p}) = P \frac{\|\mathbf{v}^H \mathbf{H}(\mathbf{p})\|^2}{\sigma^2}. \quad (9)$$

Hence, we formulate the following optimization problem

²Without loss of generality, we assume that $N_A \geq 3$.

Problem 1 (Statistical RIS beamforming):

$$\begin{aligned} \max_{\mathbf{v}} \min_{\mathbf{p} \sim f_p(\mathbf{p})} P \frac{\|\mathbf{v}^H \mathbf{H}(\mathbf{p})\|^2}{\sigma^2} \\ \text{s.t. } |v_i|^2 \leq 1 \quad \forall i, \end{aligned} \quad (10)$$

whose solution provides the RIS configuration maximizing the minimum receive SNR over the possible UE positions \mathbf{p} , which are determined by $f_p(\mathbf{p})$. However, note that Problem 1 is highly complex to tackle due to the non-convex maximization of a quadratic function in \mathbf{v} and the general expression of the UE distribution $f_p(\mathbf{p})$. In this regard, we propose to employ Monte Carlo sampling and semidefinite relaxation (SDR) in order to find a simple yet effective solution to the above problem.

Let us draw T sample points $\{\mathbf{p}_t\}_{t=1}^T$ from $f_p(\mathbf{p})$ and let $\mathbf{V} \triangleq \mathbf{v}\mathbf{v}^H$, and $\bar{\mathbf{H}}(\mathbf{p}) \triangleq \mathbf{H}(\mathbf{p})\mathbf{H}(\mathbf{p})^H$, such that Problem 1 is reformulated as

Problem 2 (Statistical RIS beamforming with SDR):

$$\max_{\mathbf{V} \succeq \mathbf{0}} \min_{\{\mathbf{p}_t\}_{t=1}^T} \text{tr}(\bar{\mathbf{H}}(\mathbf{p}_t) \mathbf{V}) \quad (12)$$

$$\text{s.t. } \text{diag}(\mathbf{V}) \leq 1 \quad (13)$$

$$\text{rank}(\mathbf{V}) = 1, \quad (14)$$

where we omit the scaling factor P/σ_n^2 as it is irrelevant for the optimization. Problem 2 can be solved in its relaxed form, i.e., when ignoring the non-convex rank constraint in Eq. (14), by employing canonical semidefinite programming such as CVX. Let \mathbf{V}^* denote the optimal solution of the relaxed version of Problem 2, then we can recover a suboptimal solution to Problem 1, namely \mathbf{v}^* , by Gaussian randomization.

Given the RIS configuration, i.e., $\Phi = \text{diag}((\mathbf{v}^*)^H)$, the DoA of the UE θ is estimated via a suitable MUSIC-based processing at the AP which is detailed as follows. However, the MUSIC procedure cannot be directly applied to the received signal \mathbf{y} in Eq. (6) since it would estimate the DoA of the equivalent uplink channel $\mathbf{G}^H \Phi^H \mathbf{h}$, which includes the target DoA θ plus the effect of the phase shift applied at the RIS and the channel path towards the AP \mathbf{G} . Moreover, the receive signal \mathbf{y} is a vector of dimension M whereas the estimation target $\mathbf{h}(\mathbf{p})$ is a vector of dimension N .³ To this end, we firstly equalize the received signal \mathbf{y} by employing minimum mean squared error (MMSE) filtering as

$$\mathbf{x}(\mathbf{p}) = \frac{1}{\sqrt{P}} \mathbf{W} \mathbf{y}(\mathbf{p}) s^* \quad (15)$$

$$= \mathbf{W} \mathbf{G}^H \Phi^H \mathbf{h}(\mathbf{p}) + \bar{\mathbf{n}} \in \mathbb{C}^N \quad (16)$$

where we set

$$\mathbf{W} \triangleq \left(\Phi \mathbf{G} \mathbf{G}^H \Phi^H + \frac{\sigma_n^2}{P} \mathbf{I}_N \right)^{-1} \Phi \mathbf{G} \in \mathbb{C}^{N \times M}, \quad (17)$$

with the equivalent noise term $\bar{\mathbf{n}} \triangleq \frac{1}{\sqrt{P}} \mathbf{W} \mathbf{n} s^*$. Note that such filtering procedure results in projecting the receive signal onto the subspace spanned by the UE channel $\mathbf{h}(\mathbf{p})$. Moreover, it

³Note that we assume $M < N$, i.e., that the number of AP antennas is less than the number of RIS elements.

does not alter the rank of said subspace, which remains equal to 1. Hence, the filtered signal $\mathbf{x}(\mathbf{p})$ can be fed to the MUSIC procedure, which estimates the direction of arrival $\hat{\theta}$ by exploiting the orthogonality between the subspace corresponding to $\mathbf{h}(\mathbf{p})$ and the noise subspace.

B. ToA Estimation

The ToA is calculated by exploiting the ideal autocorrelation property of the transmit sequences. To this end, we set the sequence $\{s(n)\}_n$ to a Constant-Amplitude Zero-Autocorrelation (CAZAC) sequence such as the Zadoff-Chu (ZC). Without loss of generality, we assume that the total transmission time L is an odd number such that we set

$$s(n) = e^{-j\pi \frac{n(n+1)}{L}}, \quad n = 1, \dots, L. \quad (18)$$

Hence, we have that the autocorrelation of the transmit signal at lag m is given by

$$R_{ss}(m) \triangleq \sum_{n=1}^L s(n)s^*(n+m) = D(m) \quad (19)$$

where $D(m)$ is the Dirac delta function. The ToA of the transmit sequence is thus estimated as $\tau = m^*/\Delta f$, where m^* is the lag corresponding to the peak in the cross-correlation matrix of the received signal with the transmit sequence $\mathbf{R}_{\mathbf{y}_s}$ and Δf is the sampling frequency.⁴ Note that since the reflection upon the RIS is instantaneous and does not increase the total ToA, the distance from the UE to the RIS d is estimated as $\hat{d} = \tau c - d_G$, where c is the speed of light. Finally, the proposed PAPIR procedure is formalized in Algorithm 1. Its complexity is dictated by the solution of the relaxed version of Problem 2, i.e., standard semidefinite programming, whose convergence is guaranteed thanks to the convex nature of the problem at hand. Overall, the proposed method is observed to converge in less than 10 iterations each one having a complexity of $\mathcal{O}(\sqrt{N}(N^6 + N^3))$.

IV. NUMERICAL RESULTS

In this section, we test the localization performance of PAPIR in a realistic scenario, in which we assume the RIS to be a squared structure with $N_x = N_y$ elements. For ease of presentation, we consider the AP, the RIS and the UE to be on the horizontal plane $z = 0$. The simulation parameters are listed in Table I, unless otherwise stated.

TABLE I: Simulation settings

Parameter	Value	Parameter	Value	Parameter	Value
M	4	N_x, N_y	4	d_G	50 m
$\psi_{D,x}$	225°	$\psi_{D,z}$	0	ψ_A	45°
P	20 dBm	σ	-80 dBm	β	2
ϵ	0.5°	N_A	3	δ	0.5
Δf	30.72 MHz	T	10 ³	Δ	0.2

Fig. 2 shows three iterations of an instance of PAPIR DoA estimation. In this example, the UE is at coordinates $\mathbf{p} =$

⁴In general, the estimation precision of the ToA can be improved by up-sampling both the received signal and the transmit sequence before computing the cross-correlation matrix between the two.

Algorithm 1 PAPIR: Passive Positioning with RIS

- 1: Data: $f_p(\mathbf{p})$, \mathcal{A} , N_A , Δ , Δf , d_G , ϵ and T
 - 2: Set $\mathcal{A}^{(1)} = \mathcal{A}$, $\epsilon > 0$, and $n = \ell = 1$
 - 3: Initialize $\hat{\theta}^{(0)} \neq \hat{\theta}^{(1)}$
 - 4: Divide $\mathcal{A}^{(1)}$ into N_A equal subareas $\{\mathcal{A}_1^{(1)}, \dots, \mathcal{A}_{N_A}^{(1)}\}$ with Δ overlap
 - 5: **while** $|\hat{\theta}^{(n-1)} - \hat{\theta}^{(n)}| > \epsilon$ **do**
 - 6: **for** $\ell = 1, \dots, N_A$ **do**
 - 7: Calculate $f_p^{(n)}(\mathbf{p})$ over the subarea $\mathcal{A}_\ell^{(n)}$
 - 8: Draw T points $\{\mathbf{p}_t\}_{t=1}^T$ according to $f_p^{(n)}(\mathbf{p})$
 - 9: Obtain \mathbf{V}^* by solving the relaxed version of Problem 2
 - 10: Obtain \mathbf{v}^* from \mathbf{V}^* via Gaussian randomization
 - 11: Set $\Phi = \text{diag}((\mathbf{v}^*)^H)$ and collect \mathbf{y}
 - 12: Set \mathbf{W} as in Eq. (17) and \mathbf{x} as in Eq. (15)
 - 13: Estimate $\hat{\theta}_\ell$ via MUSIC on the signal \mathbf{x}
 - 14: **end for**
 - 15: Define $\mathcal{A}^{(n+1)}$ as the union of the subareas corresponding to the $N_A - 1$ $\{\hat{\theta}_\ell\}_{\ell=1}^{N_A}$ that maximize the likelihood
 - 16: Set $\hat{\theta}^{(n+1)}$ as the one that maximizes the likelihood among the available $\{\hat{\theta}_\ell\}_{\ell=1}^{N_A}$
 - 17: Divide $\mathcal{A}^{(n+1)}$ into N_A equal subareas $\{\mathcal{A}_1^{(n+1)}, \dots, \mathcal{A}_{N_A}^{(n+1)}\}$ with Δ overlap
 - 18: $n \leftarrow n + 1$
 - 19: **end while**
 - 20: Calculate $\mathbf{R}_{\mathbf{y}_s}$
 - 21: Set m^* as the lag corresponding to the peak in $\mathbf{R}_{\mathbf{y}_s}$
 - 22: Set $\tau = m^*/\Delta f$
 - 23: Fix $\hat{\theta} = \hat{\theta}^{(n)}$ and $\hat{d} = \tau c - d_G$
-

$[d \cos(\theta), d \sin(\theta), 0]^T$, where $\theta \equiv \theta_x$ and $\theta_z = 0$, with $\theta_x = 300^\circ$ and $d = 70$ m. As expected, the narrower the probe areas the sharper the peaks in the respective MUSIC pseudospectrum. In particular, the last iteration returns an estimate $\hat{\theta}$ with a corresponding absolute DoA error of less than one tenth of a degree. It is worth pointing out that the pseudospectrum peak is not necessarily associated to a high estimation accuracy due to its dependency on the beamforming optimization at the RIS, whose antenna diagrams are respectively depicted in Fig. 3. Not surprisingly, the beamformers become iteratively more selective, although their overall shape is not regular, especially in the first iterations. This further motivates the choice of leveraging the prior statistical information on the UE position rather than the amplitude of the MUSIC pseudospectrum peaks, which may be affected by beamforming artifacts.

Moreover, we investigate the PAPIR overall localization accuracy in terms of root-mean-square error (RMSE). To this aim, we assume that the UE position is uniformly distributed as $f_p(\mathbf{p}) = \mathcal{U}[260^\circ, 320^\circ] \times \mathcal{U}[20 \text{ m}, 80 \text{ m}]$ and sample such distribution by drawing T points. Note that we average our simulation results over 10³ Monte Carlo runs. In Fig. 4, we depict the RMSE performance against different numbers of RIS elements $N \in \{16, 32, 64\}$ over the iterations of the

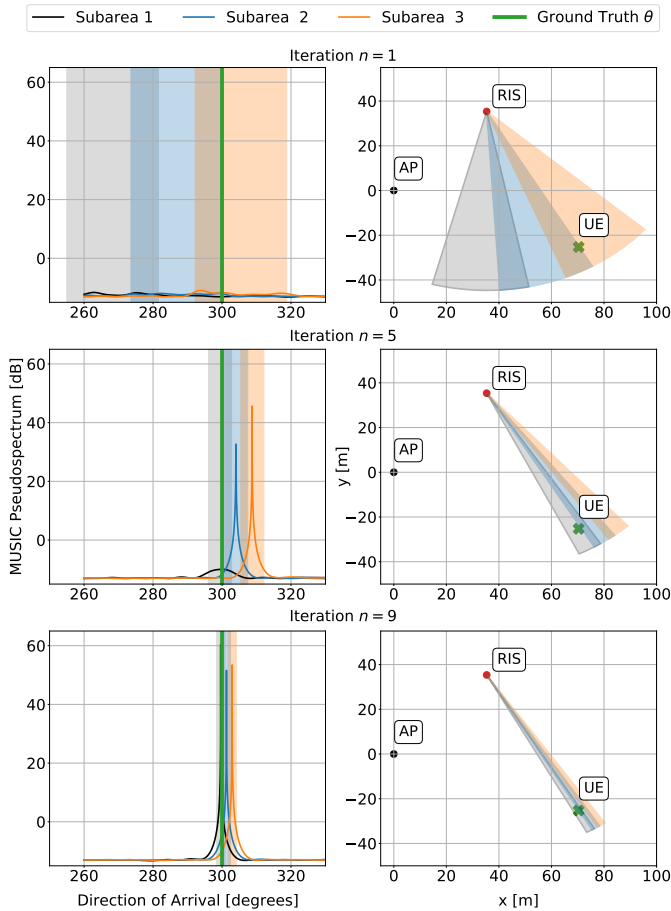


Fig. 2: One instance of PAPIR DoA estimation.

PAPIR algorithm. Although the RMSE decreases with the number of iterations for any N , the relative gain obtained by increasing N appears to have a diminishing trend, which suggests the existence of a sweet spot in the RIS configuration for this particular localization problem.

V. CONCLUSIONS

In this paper we presented PAPIR, a practical localization system leveraging on RISs, which estimates UE positions by performing statistical beamforming, DoA and ToA estimation on a given three-dimensional search space. To the best of our knowledge, PAPIR is the first two-stage localization solution employing a fully-passive single-RIS in reflection mode. PAPIR takes advantage of prior statistical information on the UE position to optimize the RIS reflection coefficients as to probe a given search space, which is iteratively updated on the basis of the likelihood of the UE position.

VI. ACKNOWLEDGEMENTS

This work has been supported by EU H2020 RISE-6G project (grant number 101017011).

REFERENCES

[1] M. Di Renzo *et al.*, “Smart Radio Environments Empowered by Reconfigurable Intelligent Surfaces: How It Works, State of Research, and The Road Ahead,” *IEEE J. Sel. Areas Commun.*, vol. 38, no. 11, pp. 2450–2525, 2020.

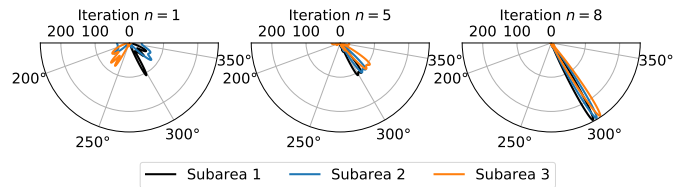


Fig. 3: Antenna diagram of the RIS configuration for different iterations of one instance of the PAPIR DoA estimation.

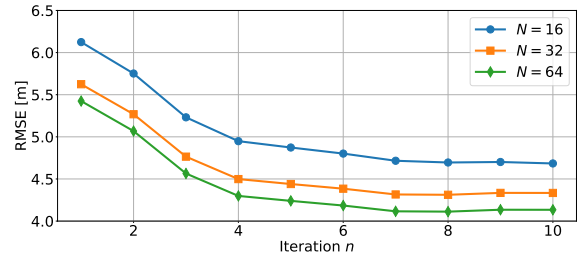


Fig. 4: Overall PAPIR localization accuracy in terms of RMSE against iterations.

[2] Q. Wu and R. Zhang, “Towards Smart and Reconfigurable Environment: Intelligent Reflecting Surface Aided Wireless Network,” *IEEE Commun. Mag.*, vol. 58, no. 1, pp. 106–112, 2020.

[3] P. Mursia *et al.*, “RISMA: Reconfigurable Intelligent Surfaces Enabling Beamforming for IoT Massive Access,” *IEEE J. Sel. Areas Commun.*, vol. 39, no. 4, pp. 1072–1085, 2020.

[4] E. Calvanese Strinati *et al.*, “Wireless Environment as a Service Enabled by Reconfigurable Intelligent Surfaces: The RISE-6G Perspective,” *Proceedings of EuCNC 6G Summit*, 2021.

[5] P. Mursia *et al.*, “RISE of Flight: RIS-Empowered UAV Communications for Robust and Reliable Air-to-Ground Networks,” *IEEE Open J. Commun. Soc.*, pp. 1–1, 2021.

[6] H. Wymeersch and B. Denis, “Beyond 5G Wireless Localization with Reconfigurable Intelligent Surfaces,” in *Proc. IEEE Int. Conf. Commun. (ICC)*, 2020, pp. 1–6.

[7] H. Wymeersch *et al.*, “Radio Localization and Mapping With Reconfigurable Intelligent Surfaces: Challenges, Opportunities, and Research Directions,” *IEEE Veh. Technol. Mag.*, vol. 15, no. 4, pp. 52–61, 2020.

[8] J. He *et al.*, “Adaptive Beamforming Design for mmWave RIS-Aided Joint Localization and Communication,” in *Proc. IEEE Wireless Commun. and Netw. Conf. (WCNC)*, 2020, pp. 1–6.

[9] A. Fascista *et al.*, “RIS-aided Joint Localization and Synchronization with a Single-Antenna MmWave Receiver,” 2020. [Online]. Available: <https://arxiv.org/abs/2010.14825>

[10] S. Hu *et al.*, “Beyond Massive MIMO: The Potential of Positioning With Large Intelligent Surfaces,” *IEEE Trans. Signal Process.*, vol. 66, no. 7, pp. 1761–1774, 2018.

[11] T. Ma *et al.*, “Indoor Localization With Reconfigurable Intelligent Surface,” *IEEE Commun. Lett.*, vol. 25, no. 1, pp. 161–165, 2021.

[12] F. Guidi and D. Dardari, “Radio Positioning with EM Processing of the Spherical Wavefront,” *IEEE Trans. Wireless Commun.*, pp. 1–1, 2021.

[13] A. Elzanaty *et al.*, “Reconfigurable Intelligent Surfaces for Localization: Position and Orientation Error Bounds,” 2020. [Online]. Available: <https://arxiv.org/abs/2009.02818>

[14] J. He *et al.*, “Large Intelligent Surface for Positioning in Millimeter Wave MIMO Systems,” in *IEEE Veh. Tech. Conf. (VTC)*, 2020, pp. 1–5.

[15] H. Zhang *et al.*, “Towards Ubiquitous Positioning by Leveraging Reconfigurable Intelligent Surface,” *IEEE Commun. Lett.*, vol. 25, no. 1, pp. 284–288, 2021.

[16] C. L. Nguyen *et al.*, “Reconfigurable Intelligent Surfaces and Machine Learning for Wireless Fingerprinting Localization,” 2020. [Online]. Available: <https://arxiv.org/abs/2010.03251>

[17] S. Abeywickrama *et al.*, “Intelligent Reflecting Surface: Practical Phase Shift Model and Beamforming Optimization,” *IEEE Trans. Commun.*, vol. 68, no. 9, pp. 5849–5863, 2020.